PL-TR-94-2044

MOLECULAR NITROGEN FLUORESCENCE LIDAR FOR REMOTE SENSING OF THE AURORAL IONOSPHERE

Richard Garner
Michael Burka

PhotoMetrics, Inc.
4 Arrow Drive
Woburn, MA 01801-2067

24 February 1994

Scientific Report No. 1

PHILLIPS LABORATORY
DIRECTORATE OF GEOPHYSICS
AIR FORCE MATERIEL COMMAND
HANSCOM AFB, MA 01731-3010

"This technical report has been reviewed and is approved for publication"

PHAN DAO
Contract Manager

DAVID ANDERSON
Branch Chief

WILLIAM K. VICKERY
Division Director

This report has been reviewed by the ESC Public Affairs Office (PA) and is releasable to the National Technical Information Service (NTIS).

Qualified requestors may obtain additional copies from the Defense Technical Information Center (DTIC). All others should apply to the National Technical Information Service (NTIS).

If your address has changed, if you wish to be removed from the mailing list, or if the addressee is no longer employed by your organization, please notify PL/TSI, 29 Randolph Road, Hanscom AFB, MA 01731-3010. This will assist us in maintaining a current mailing list.

Do not return copies of this report unless contractual obligations or notices on a specific document requires that it be returned.

REPORT DOCUMENTATION PAGE

Form Approved OMB No. 0704-0188

1. AGENCY USE ONLY *(Leave blank)*	2. REPORT DATE	3. REPORT TYPE AND DATES COVERED
	24 February 1994	Scientific Report No. 1

4. TITLE AND SUBTITLE
Molecular Nitrogen Fluorescence Lidar for Remote Sensing of the Auroral Ionosphere

5. FUNDING NUMBERS
PE 63402F
PR 2295 TA 24 WU AB

Contract F19628-92-C-0160

6. AUTHOR(S)
Richard Garner
Michael Burka

7. PERFORMING ORGANIZATION NAME(S) AND ADDRESS(ES)
PhotoMetrics, Inc.
4 Arrow Drive
Woburn, MA 01801-2067

8. PERFORMING ORGANIZATION REPORT NUMBER

9. SPONSORING/MONITORING AGENCY NAME(S) AND ADDRESS(ES)
Phillips Laboratory
29 Randolph Road
Hanscom AFB, MA 01731-3010
Contract Manager: Phan Dao/GPIM

10. SPONSORING/MONITORING AGENCY REPORT NUMBER
PL-TR-94-2044

11. SUPPLEMENTARY NOTES

12a. DISTRIBUTION/AVAILABILITY STATEMENT
Approved for Public Release; Distribution Unlimited

12b. DISTRIBUTION CODE

13. ABSTRACT *(Maximum 200 words)*

We describe two types of molecular nitrogen fluorescence lidars which can be used to determine excited or ionized N_2 density in the ionosphere during moderate or strong aurora. The lidars can also be used for high spatial resolution diagnostics during ionospheric high power radio frequency heating experiments which are often performed when there is moderate auroral activity. The lidars excite N_2 already excited or ionized through impact with high energy auroral electrons. Several different configurations are considered for each lidar. The first type of lidar is a conventional fluorescence lidar which operates in the first postive system ($N_2(A^3\Sigma_u^+) \longrightarrow N_2(B^3\Pi_g)$) or the first negative system ($N_2^+(X^2\Sigma_g^+) \longrightarrow N_2^+(B^2\Sigma_u^+)$). Several different lasers are considered. The choice of laser determines the bands for excitation and fluorescence. The second type of lidar first pumps excited N_2 to a higher energy state and then does conventional fluorescence lidar on that state. This lidar utilizes two lasers. The first laser, the pump laser, operates in the first positive system. The second laser, the probe laser, operates in the second positive system ($N_2(B^3\Pi_g) \longrightarrow N_2(C^3\Pi_u)$). Both lidars are described in detail and results of signal to noise calculations are performed using reasonable system parameters.

14. SUBJECT TERMS
lidar; auroral lidar; ionospheric lidar; fluorescence lidar; nitrogen fluorescence

15. NUMBER OF PAGES
40

16. PRICE CODE

17. SECURITY CLASSIFICATION OF REPORT	18. SECURITY CLASSIFICATION OF THIS PAGE	19. SECURITY CLASSIFICATION OF ABSTRACT	20. LIMITATION OF ABSTRACT
UNCLASSIFIED	UNCLASSIFIED	UNCLASSIFIED	SAR

Contents

List of Figures

List of Tables

Acknowledgements

Dr. Phan Dao, the contract manager, provided valuable contributions during the course of this work.

We thank Dr. Ralph Wuerker, Dr. Alfred Wong, and Mr. Tetsuo Fukuchi, all of the UCLA Plasma Physics Laboratory, for helpful discussions in the preparation of this report. Dr. Wuerker, Dr. Wong, and Mr. Fukuchi were also involved in the collaborative effort between UCLA and PL/GPIM described in Appendix Appendix B.

1 Introduction

We describe two types of molecular nitrogen fluorescence lidars which can be used to probe the D region of the ionosphere during periods of moderate or strong auroral activity. Both types of lidars measure, as a function of altitude, the density of a particular excited or ionized state of N_2. Excited and ionized states of N_2 exist in aurora due to impact of ground state N_2 with high energy electrons.

The lidars can also be used for high spatial resolution diagnostics during ionospheric high power radio frequency heating experiments. In this application both lidars utilize the fact that ionospheric heating experiments are often performed during periods of moderate auroral activity. Moderate auroral activity is necessary for there to be generation of ELF and VLF radiation by ionospheric electrons during rf heating [1]. During the application of high power rf the temperature of the electrons increases which in turn causes changes in the densities of excited and ionized N_2 states. The lidars then detect the changes in density of a particular excited or ionized state. Changes in electron temperature are then inferred from these changes in density.

The first type of lidar we describe is a conventional laser induced fluorescence (LIF) lidar operating in the 1^{st} positive system ($N_2(A^3\Sigma_u^+) \rightarrow N_2(B^3\Pi_g)$) or the 1^{st} negative system ($N_2^+(X^2\Sigma_g^+) \rightarrow N_2^+(B^2\Sigma_u^+)$) of molecular nitrogen (see the enery level diagram for N_2 in Figure 1). Several different excitation/fluorescence wavelength combinations are considered, depending on the choice of laser.

The second type of lidar we refer to as a pump/LIF lidar. Two lasers are used. The first laser, the so-called pump laser, pumps the excited nitrogen from $N_2(A^3\Sigma_u^+)$ to $N_2(B^3\Pi_g)$ (1^{st} positive system). The second laser, the so-called probe laser, is then used to do LIF lidar on the 2^{nd} positive system ($N_2(B^3\Pi_g) \rightarrow N_2(C^3\Pi_u)$). As a comparison we show that a conventional LIF lidar operating in the 2^{nd} positive system without a 1^{st} positive pump is not viable for D region studies.

We consider several different lasers for both types of lidars. Figure 2 is a schematic of an energy level diagram showing four different lidar scenarios. We will consider these four scenarios throughout this report. The first three scenarios refer to LIF lidars and the fourth refers to a pump/LIF lidar. For each scenario is list of lasers we consider and their nominal wavelengths.

All lasers of both lidars can be nitrogen lasers operating in the band of interest [2].

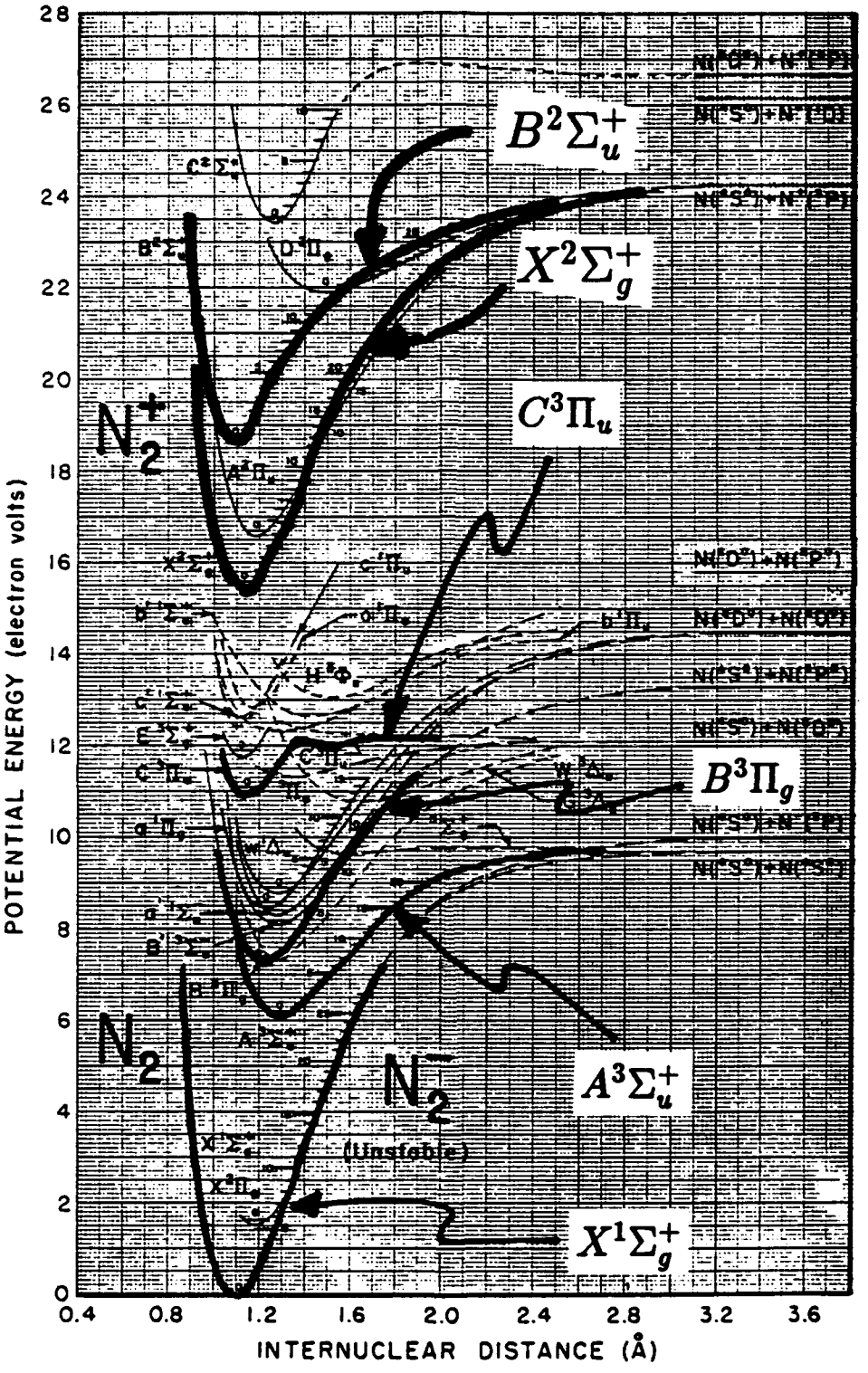

Figure 1: Energy levels of molecular nitrogen [12]. The electronic states of interest in this report are highlighted.

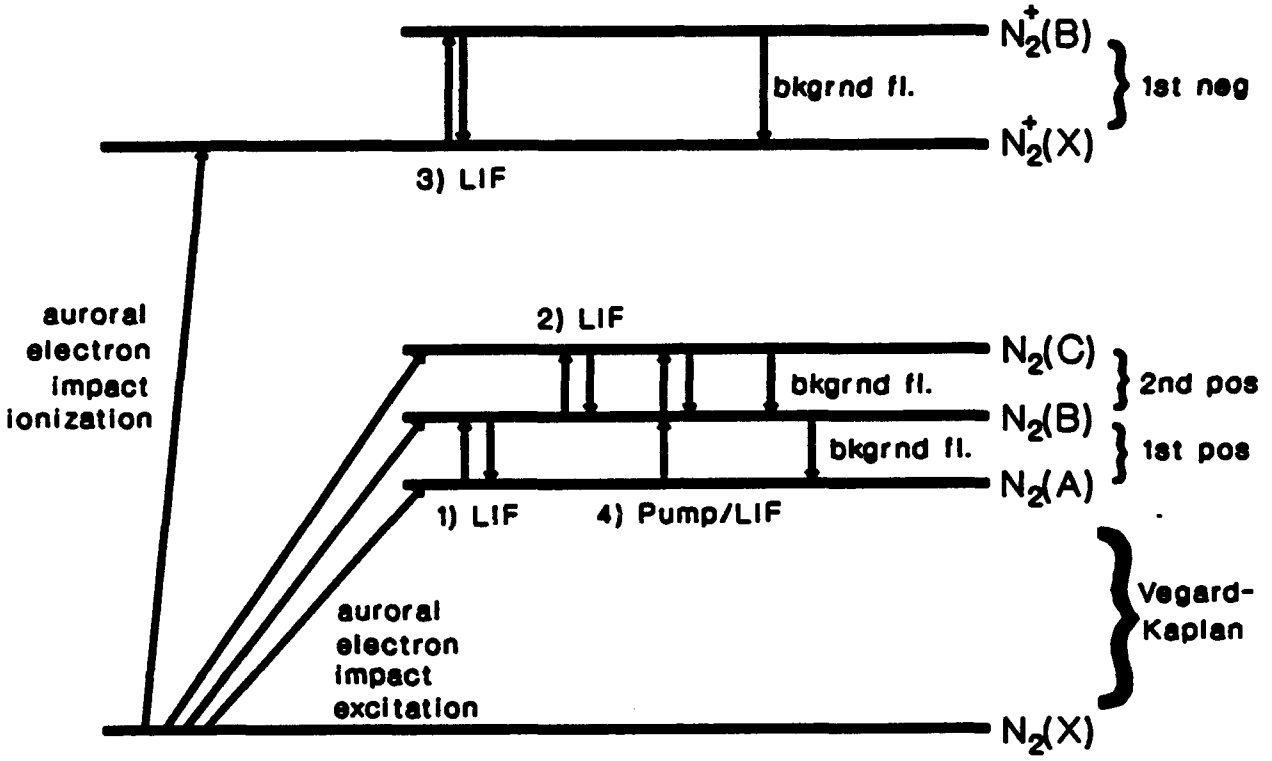

Lasers and (excitation,fluorescence) wavelengths

1) dye (7737,7737)
N2 (7737,7737)
Nd:YAG (10644,7484)
Ti:Sapphire (7737,7737)

2) N2 (3371,3371)
dye (3371,3371)

3) dye (3914,3914)
Ti:Sapphire (3914,3914)

4) pump: dye (10477)
Nd:YLF (10472)
LIF: N2 (3371,3371)

Figure 2: Four lidar scenarios (first three: LIF; fourth: pump/LIF), the lasers considered for each, and the nominal wavelengths at which they operate.

This precludes the need for wavelength tuning. Alternatively, for the 1^{st} positive system we consider tunable dye and Ti:Sapphire lasers, and nontunable Nd:YAG and Nd:YLF lasers. The latter two lasers happen to operate at wavelengths which coincide with specific rotational transitions of the 1^{st} positive system (see Figure 2). Since the Phillips Laboratory/Ionospheric Effects division (PL/GPIM) mobile lidar is equipped with a Nd:YAG, this type of laser is an especially attractive choice. For the 1^{st} negative and 2^{nd} positive systems we consider dye and Ti:Sapphire lasers.

In addition to detecting fluorescence both types of lidars can simultaneously detect elastic (Rayleigh) backscattered laser radiation from air molecules as a function of altitude up to and including the D region [3]. This provides density measurements of the ambient atmosphere. Then, with standard lidar techniques, the temperature of the ambient atmosphere can be deduced from these density measurements. The elastic lidar can be used to monitor gravity wave activity at D region altitudes which may have significant effects on ionospheric heating [4].

Due to the relatively small beam divergence of a lidar, high horizontal spatial resolution can be achieved as well with a scannable lidar system.

We discuss both types of lidars in detail in the following sections. We present signal to noise calculations and we discuss the reasons for choosing the various transitions and the relative merits of each type of lidar. The results of our signal to noise calculations are compiled in Table 8 on page 19.

Sections 2 and 3 discuss LIF lidar and pump/LIF lidar respectively. Both sections present a general description of each lidar and show how number of detected photons is calculated.

Section 4 shows how the density of the aurorally excited or ionized molecular nitrogen is calculated. These densities are required for determining number of signal photons. The density calculations are based on observed column emission data from aurora.

Section 5 discusses signal to noise ratio and presents results of signal to noise calculations. Section 5.1 presents the number of photons expected for each lidar scenario that we consider. All the necessary lidar parameters required for this calculation are listed. Section 5.2 discusses and quantifies the noise processes that we consider. Section 5.3 then presents signal to noise ratios for each lidar scenario.

Appendix Appendix A shows how we calculate wavelengths of individual rotational lines of N_2 and N_2^+.

Appendix Appendix B summarizes laboratory based laser induced fluorescence experiments performed at the UCLA Plasma Physics Laboratory in February, 1993.

Appendix Appendix C shows passive emission data acquired with the receiver of PL/GPIM mobile lidar system at the HIPAS observatory in Alaska.

2 LIF Lidar

2.1 General Description

The LIF lidars that we consider use a narrow band laser to excite D region molecular nitrogen from a single rotational level of a specific vibrational level of a specific electronic state to another rotational level of a specific vibrational level of a higher energy electronic state. The molecule then decays (fluoresces) to a rotational and vibrational level of the original electronic state. The lower rotational and vibrational levels may or may not be identical to the original ones. Also, the lower electronic state is an excited state of N_2 or a state of N_2^+. A telescope situated adjacent to the laser detects the fluorescence radiation.

In designing a LIF lidar consideration must be given to the electronic system (i.e, electronic transition), the excitation and fluorescence bands within the electronic system (i.e., vibrational transitions), and the excitation and fluorescence rotational transitions.

Electronic system

The choice of electronic system is driven by the need for a practical wavelength, a strongly absorbing and radiating system, and a relatively high density of the lower electronic state. We consider LIF lidars operating in the 1^{st} positive, 1^{st} negative, and 2^{nd} positive systems. The 1^{st} positive system, which has wavelengths from the visible red to the mid infrared, is considered because of the relatively high number density of $N_2(A^3\Sigma_u^+)$ in the D region during an aurora. The density of $N_2(A^3\Sigma_u^+)$ is high because of its relatively long lifetime at D region altitudes. For example, at 100 km the lifetime of $N_2(A^3\Sigma_u^+)$ is approximately 45 msec. The dominant loss mechanisms are due to collisional quenching with O and O_2. (As a comparison, the radiative lifetime of $N_2(A^3\Sigma_u^+)$ is 2 sec.) The density of $N_2(A^3\Sigma_u^+)$ is derived in Section 4.

We consider the 1^{st} negative system, which has wavelengths from the near UV to the blue visible, because of the relatively high absorption cross sections and Franck-Condon factors of some bands in this system. Also, the density of $N_2^+(X^1\Sigma_g^+)$ is relatively high,

although not as high as the density of $N_2(A^3\Sigma_u^+)$.

A LIF lidar operating in the 2^{nd} positive system, which has wavelengths from the far UV to near UV, is not viable for D region studies because of the very low number density of $N_2(B^3\Pi_g)$. The density of $N_2(B^3\Pi_g)$ is low because of its relatively short radiative lifetime of approximately 10 μsec. However, because of the high density of $N_2(A^3\Sigma_u^+)$ the 2^{nd} positive system can be used in LIF lidar if some $N_2(A^3\Sigma_u^+)$ molecules are first excited to $N_2(B^3\Pi_g)$. This is the basic idea of a pump/LIF lidar discussed in the next section. Here we present conventional 2^{nd} positive LIF lidar as a comparison.

Lower vibrational and rotational levels of excitation transition

The lower vibrational and rotational states of the excitation transition are chosen, where possible, to be those which are most abundant at D region altitudes during aurora. For the situations in which the lasers are not tunable (i.e., Nd:YAG and Nd:YLF) the vibrational and rotational levels are pre-determined by the laser wavelength. For the situations in which a nitrogen laser is used there may be several lower rotational levels excited, depending on the laser output. In some situations the most abundant vibrational state may not be well coupled to an upper state (i.e., low absorption cross section) and an alternative lower vibrational state must be considered.

The density of a vibrational state of an electronic system is determined from past observations of aurora reported in the literature [5]. Section 4 describes how we calculate the density from these observations.

The density of a rotational level is determined by assuming the rotational states of a given vibrational level to be in thermal equilibrium with the surroundings. In this case the fraction of molecules $R_{e,v}(J)$ in electronic state e and vibrational state v that are in rotational state J at temperature T is [6]

$$R_{e,v}(J) = \frac{hcB_v}{kT}(2J+1)\exp\left[-\frac{hcB_vJ(J+1)}{kT}\right] \qquad (1)$$

where the constant B_v is a function of spectroscopic constants and the vibrational quantum number (see Appendix Appendix A).

Upper vibrational and rotational levels and
lower vibrational and rotational levels of the fluorescence transition

Ideally, the upper vibrational level and the lower vibrational level of the fluorescence

transtion are chosen to be those levels which give the greatest product of absorption cross section and Franck-Condon factor. The former is proportional to the strength of the excitation transition and the latter is proportional to the strength of the fluorescence transition. In reality, however, consideration must be given to the wavelengths of both transitions and to the lifetime of the upper state. The choice of excitation wavelength is driven by the choice of laser. The choice of fluorescence wavelength is driven by the choice of detector. The radiative lifetime of the upper state limits the vertical resolution of the lidar. Nonradiative quenching of the upper state decreases the number of photons that would otherwise be produced by fluorescence.

The upper rotational level and the lower rotational level of the fluorescence transition are almost determined after the lower rotational level of the excitation transtion is chosen. The rotational transition must obey the selection rule $\Delta J = 0, \pm 1$, with the condition that $\Delta J = 0$ is forbidden for electronic systems in which both states have zero angular momentum along the internuclear axis.[1] The transition $J = 0 \longrightarrow J = 0$ is always forbidden. Transitions with $\Delta J = J_{upper} - J_{lower} = -1$ are in the P branch, $\Delta J = +1$ are in the R branch, and $\Delta J = 0$ are in the Q branch.

After the upper rotational level of the excitation transtition is chosen from two, or in some cases three, possible choices, the lower rotational level of the fluorescence transition can be chosen so that the lidar detects any combination of the two (or three) fluorescing branches. The filter in the lidar receiver determines which brancnes are detected. If the bandwidth of the filter is wide enough (perhaps on the order of 10–30 Å) then all branches can be detected and the signal is two (or three) times higher than it would otherwise be if detecting only one branch. However, there is a tradeoff because a wide bandwidth filter allows more background radiation to be detected.

Figure 3 shows the four lidar scenarios along with the list of lasers and the specific electron/vibrational/rotational transitions that we consider for each. The excitation and fluorescence wavelengths are also shown. The wavelengths are calculated using spectroscopic constants from Ref. [7]. Appendix Appendix A describes these calculations in detail.

[1] In the parlance of molecular spectroscopy such a state is designated by Σ. For example, the 1^{st} negative system refers to transtions from $N_2^+(X^2\Sigma_g^+)$ to $N_2^+(B^2\Sigma_u^+)$. Both states are Σ states and therefore $\Delta J \neq 0$.

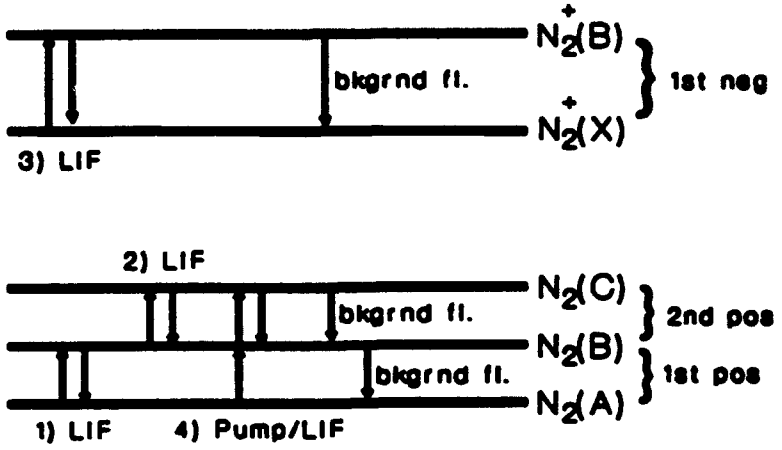

1) Ti-Saph,dye: v=0,J=6 --> v=2,J=5 --> v=0,J=4,5,6
(7736.5) (7717.3) (7726.3) (7736.5)
N2: v=0 --> v=2 --> v=0
(7737) (7737)
Nd:YAG: v=5,J=12 --> v=4,J=13 --> v=2,J=12,13,14
(10647) (7445.9) (7466.2) (7488.3)

2) N2: v=0 --> v=0 --> v=0
(3371) (3371)
dye: v=0,J=6 --> v=0,J=5 --> v=0,J=4,5,6
(3371.9) (3367.9) (3369.7) (3371.9)

3) dye: v=1,J=6 --> v=0,J=5 --> v=0,J=4,6
(3914.3) (3907.8) (3914.3)

4) pump: dye: v=0,J=6 --> v=0,J=5
(10476.3)
Nd:YLF: v=0,J=3 --> v=0,J=2
(10472.0)
LIF: N2: v=0 --> v=0 --> v=0
(3371) (3371)

Figure 3: Specific transitions and the corresponding wavelengths for the four lidar scenarios.

2.2 LIF Lidar Signal

For the conventional LIF lidar the number of photons $n_{sig}(r)$ detected per laser pulse by the lidar receiver in a time period Δt, at a time $t = 2r/c$ after the start of a laser pulse is

$$n_{sig}(r) = \eta K \frac{E_o \lambda}{hc} K \frac{\frac{\pi}{4} D_r^2}{r^2} N_{e,v} R_{e,v}(J) G F_{e'-e''}^{v'-v''} \frac{\sigma_{e'-e''}^{v'-v''} Q}{4\pi} T_u(r) T_d(r) \Delta r \Gamma(r). \qquad (2)$$

This equation assumes: 1) the fluorescence medium is not saturated, and 2) the spectral shape of the laser radiation is approximately the same as the spectral shape of the excitation.

Each factor in Eq. 2 is described below.

- η is the quantum efficiency of the detector.
- K is the transmissivity of the receiver optics.
- E_o is the laser energy per pulse.
- D_r is the diameter of the telescope aperture.
- $N_{e,v}$ is the density of N_2 or N_2^+ in electronic state e and vibrational state v (the species to be excited).
- $R_{e,v}(J)$ is the fraction of the $N_{e,v}$ molecules which are in rotational state J (see Eq. 1 above).
- $F_{e'-e''}^{v'-v''}$ is the Franck-Condon factor associated with a transition from electronic/vibrational state e'/v' to electronic/vibrational state e''/v'' (i.e., the probability that $N_2(e', v')$ decays to $N_2(e'', v'')$ instead of other vibrational states).
- G is the fraction of fluorescence radiation that is within the bandwidth of the receiver.
- $\sigma_{e'-e''}^{v'-v''}$ is the absorption cross section for absorption of a photon by a molecule in the electronic/vibrational state e''/v'' to produce a molecule in the electronic/vibrational state e'/v'. The absorption cross section is calculated in the following way:

$$\sigma_{e'-e''}^{v'-v''} = \frac{A\lambda^2}{8\pi\Delta\nu} \quad \text{(mks units)}, \qquad (3)$$

where

  - A is the transition probability,

- λ is the wavelength of the transition, and
- $\Delta\nu$ is the bandwidth of the transition (primarily doppler).

- Q is the quenching factor for nonradiative decay of the excited molecule.
- The factor 4π indicates that fluorescence emission is assumed isotropic.
- $T_u(r)$ and $T_d(r)$ are the transmissivities of the atmosphere from the lidar up to range r at the wavelengths of the upwardly propagating and downwardly propagating radiation, respectively.
- $\Delta r = c\Delta t/2$, where Δt is the integration time of the detector.
- $\Gamma(r)$ is the fluorescence lifetime correction factor [6]. This factor, which is a dimensionless quantity less than or equal to unity, is present due to the nonzero lifetime of the excited state and the fact that the lidar return at time $t = 2r/c$ may be due to photons from ranges less than r as well. This factor approaches unity as the distance into the fluorescence medium increases. For fluorescence lifetimes short compared to detector integration time this factor is near unity for all range points.

Section 5 presents lidar parameters and results of calculations for numbers of photons detected by hypothetical LIF lidars (see Table 6).

3 Pump/LIF Lidar

3.1 General Description

The pump/LIF lidar is similar to a conventional LIF lidar. However the excited species that it probes, in an LIF lidar manner, is created by first laser pumping from a lower state. This lidar utilizes two lasers. The first laser, the so-called pump laser, excites nitrogen from $N_2(A^3\Sigma_u^+)$ to $N_2(B^3\Pi_g)$ (1^{st} positive system). The second laser, the so-called the probe laser, excites nitrogen from $N_2(B^3\Pi_g)$ to $N_2(C^3\Pi_u)$ (2^{nd} positive system). The receiver detects fluorescence from $N_2(C^3\Pi_u)$ to the $N_2(B^3\Pi_g)$.

The impetus for this type of lidar is the desirability of doing LIF lidar on the 2^{nd} positive system. Such a lidar detects radiation in the near UV for which higher quantum efficiency photomultiplier tubes exist. Unfortunately, the density of $N_2(B^3\Pi_g)$ that exists during moderate aurora is too low for this type of lidar by itself to be feasible. However,

the density of $N_2(A^3\Sigma_u^+)$ is quite high. Therefore, another laser is used to create $N_2(B^3\Pi_g)$ from the abundance of $N_2(A^3\Sigma_u^+)$.

Another advantage of the pump/LIF lidar becomes evident after calculating the number of photons expected to be detected. The number of photons detected is proportional to the inverse of the square of the laser divergence, if the divergences of both lasers are the same. (If the divergences of the pump and probe lasers are different, then take the larger of the two divergences).[2] This property of the pump/LIF lidar allows for the increase of the signal by placing beam expanders on the outputs of the lasers. The only limitation is the diffraction limit of the beam expanders (i.e., the size of the beam expander aper

Similar issues guide the choice of transitions for the pump/LIF lidar as those that g... the choice for the conventional LIF lidar. The pump/LIF lidar has the pump transition (induced by the pump laser), the excitation transition (induced by the probe laser), and the fluorescence transition (detected by the receiver). Figure 3 shows the specific transitions that we consider. In that figure the pump/LIF lidar is depicted as scenario number four.

3.2 Pump/LIF Lidar Signal

For the pump/LIF lidar the number of photons $n_{sig}(r)$ detected per laser pulse by the lidar receiver in a time period Δt, at a time $t = 2r/c$ after the start of a laser pulse is

$$n_{sig}(r) = \eta K \frac{1}{\frac{\pi}{4}(r\theta_l)^2} \frac{E_A E_B \lambda_{AB} \lambda_{BC}}{(hc)^2} N_{A,v_p} \sigma_{AB}^{v''-v_p} F_{C-B}^{v'-v''} G \frac{\sigma_{BC}^{v'-v''} Q}{4\pi} \frac{\frac{\pi}{4} D_r^2}{r^2} T_p(r) T_l(r) T_u(r) \Gamma(r) \Delta r \tag{4}$$

In Eq. 4 A, B, and C refer to the three electronic levels involved in the pump/LIF process. The pump laser pumps from A to B. The probe laser excites from B to C. The receiver detects fluorescence radation from the decay of C to B. Each factor in Eq. 4 which does not also occur in Eq. 2 is described below. Factors which are also in Eq. 2 are described in the text after that equation.

- θ_l is the laser divergence. Equation 4 assumes both lasers to matched (i.e., same divergences).
- E_A is the laser energy per pulse of the pump laser.
- E_B is the laser energy per pulse of the probe laser.

[2]For a conventional LIF lidar the number of photons detected is independent of the laser divergence as long as the receiver field of view completely encompasses the laser beam.

- λ_{AB} is the wavelength corresponding to the pump transition.
- λ_{AB} is the wavelength corresponding to the fluorescence transition.
- N_{A,v_p} is the density of $N_2(A, v_p)$, the state excited by the pump laser. v_p is the vibrational level.
- $R_{A,v_p}(J_p)$ is the fraction of the N_{A,v_p} molecules which are in rotational state J_p (see Eq. 1 above).
- $\sigma_{AB}^{v'-v_p}$ is the absorption cross section for the pump transition. The absorption cross section is calculated using Eq. 3.
- $\sigma_{BC}^{v'-v''}$ is the absorption cross section for the excitation transition.
- $F_{BC}^{v'-v''}$ is the Franck-Condon factor associated with fluorescence transition vibrational band.
- G is the fraction of fluorescence radiation that is within the bandwidth of the receiver.
- $T_p(r)$, $T_l(r)$, and $T_u(r)$ are the transmissivities of the atmosphere from the lidar up to range r for the pump, excitation, and fluorescence wavelengths, respectively.

Section 5 presents lidar parameters and results of calculations for numbers of photons detected by hypothetical pump/LIF lidars (see Table 6).

4 Density of Excited and Ionized Molecular Nitrogen

The calculation of LIF or pump/LIF lidar signals requires knowledge of the density of the specific vibrational state that is to be excited (LIF lidar) or pumped (pump/LIF lidar). The fraction of these that are in a specific rotational state is then calculated with Eq. 1. The density of a vibrational state that radiatively decays to other states can be derived from observed column emission rates, of the relevant bands, from aurora. The density of a state that does not radiatively decay (e.g., $N_2^+(X^2\Sigma_g^+)$) requires a different technique, which we describe below. Of all the lidar scenarios that we consider (see Figure 3) only one, the 1^{st} negative LIF lidar, requires knowledge of the density of a nonradiative state.

4.1 Density of Excited N_2

The 1st positive, 2nd positive, and pump/LIF lidars depicted in Figure 3 involve exciting $N_2(A^3\Sigma_u^+)$ or $N_2(B^3\Pi_g)$. The densities of specific vibrational states of $N_2(A^3\Sigma_u^+)$ can be derived from observed column emission rates of the relevant bands in the Vegard-Kaplan system. The densities of specific vibrational states of $N_2(B^3\Pi_g)$ can be derived from observed column emission rates of the relevant bands in the 1st postive system. Column emission rates for type IBC3 aurora are reported in Reference [5]. The relevant bands are all those which have an upper vibrational level identical to the vibrational level of the molecule to be excited.

For steady state conditions the density $N_{e,v}$ of N_2 in electronic state e and vibrational state v is

$$N_{e,v} = \left(\frac{1}{T} \sum_{v'} E_{e-e'}^{v-v'} \right) \tau_{e,v} \tag{5}$$

where

- $E_{e-e'}^{v-v'}$ is the column emission rate (in Rayleighs) due to the radiative decay of the electronic/vibration state e/v to the electronic/vibrational state e'/v',
- $\tau_{e,v}$ is the radiative lifetime of the e/v state, and
- T is the thickness of the aurora, which we take as 10 km.

The quantity in parentheses is the volume emission rate. Note that this calculation does not require knowledge of lifetimes associated with non-radiative decay mechanisms, which are typically difficult to estimate.

Table 1 shows the density of the N_2 states needed to calculate numbers of photons for the lidar scenarios that we consider. Also shown are the transitions that are used to determine the densities, the corresponding observed column emission rates, and the radiative lifetimes of the states.

4.2 Density of N_2^+

Here we estimate the density of $N_2^+(X^2\Sigma_g^+,v=0)$ since this is the specific vibrational state to be excited with the 1st negative LIF lidar that is depicted in Figure 3.

Since $N_2^+(X^2\Sigma_g^+,v=0)$ does not radiatively decay we cannot use the above technique to calculate its density. Instead, we estimate the ratio of the density of $N_2^+(X^2\Sigma_g^+,v=0)$ to the

LIF excitation transition[1]	relevant auroral transition[1]	column emission rate (kR)	radiative lifetime (sec)	density (cm^{-3}) (lower state of LIF trans.)[2]
1P: $(A, v=0) \rightarrow (B, v=2)$	VK: $(A, v=0) \rightarrow (X, \text{all } v)$	10	2	2×10^4
1P: $(A, v=5) \rightarrow (B, v=4)$	VK: $(A, v=5) \rightarrow (X, \text{all } v)$	2.4	2	5×10^3
2P: $(B, v=0) \rightarrow (C, v=0)$	1P: $(B, v=0) \rightarrow (A, \text{all } v)$	77	9×10^{-6}	0.7

[1]all states are of N_2 [2]assume 10 km aurora thickness

Table 1: Densities of N_2 vibrational states to be excited by the considered lidars. All parameters used to calculate the densities are included.

density of $N_2^+(B^2\Sigma_u^+)$ and then calculate the density of $N_2^+(B^2\Sigma_u^+)$, which does radiatively decay.

In the aurora N_2^+ is produced primarily by electron impact ionization of ground state N_2. N_2^+ losses are due primarily to reactions with O and O_2 (see Table 2). In steady state the density N_{z+} of $N_2^+(X^2\Sigma_g^+)$ is then simply product of the electron impact ionization production rate and the loss time due to all mechanisms:[3]

$$N_{z+} = N_o \langle \sigma_{z+}^{e^-} v \rangle \tau_{z+} \tag{6}$$

where

- N_o is the density of ground state N_2,
- $N_o\langle\sigma_{z+}^{e^-}v\rangle$ is the production rate due to electron impact ionization of ground state N_2 (v is the relative speed between the impacting electron and the molecule, $\sigma_{z+}^{e^-}$ is the differential cross section, a function of v, and $\langle\cdots\rangle$ denotes an average with respect to the velocity destribution function), and
- τ_{z+} is the loss time of $N_2^+(X^2\Sigma_g^+)$ due to all loss mechanisms.

The density $N_{z+,v=0}$ of the specific vibrational state $N_2^+(X^2\Sigma_g^+,v=0)$ is then approximately

$$N_{z+,v=0} = N_{z+} F_{z+-z}^{0-0} \tag{7}$$

where F_{z+-z}^{0-0} is the Franck-Condon factor for the transition $N_2(X^1\Sigma_g^+,v=0) \longrightarrow N_2^+(X^2\Sigma_g^+,v=0)$.[4]

[3]This disregards spatial tranport processes and production due to electron impact of other states besides ground state N_2. We assume these two effects to be small.

[4]Disregards production of $N_2^+(X^2\Sigma_g^+,v=0)$ due to electron impact with $N_2^+(X^2\Sigma_g^+,v\neq0)$.

The density N_{b+} of $N_2^+(B^2\Sigma_u^+)$ is approximately

$$N_{b+} = N_o \langle \sigma_{b+}^{e^-} v \rangle \tau_{b+} \tag{8}$$

where each variable is analogous to the corresponding one in Eq. 6. τ_{b+}, the loss time of $N_2^+(B^2\Sigma_u^+)$, is due primarily to radiative decay.

Since $N_2^+(B^2\Sigma_u^+)$ radiatively decays its density is also determined by the technique described in the last section. Therefore, N_{b+} is also written as

$$N_{b+} = \left(\frac{1}{T} \sum_{v'',v'} E_{b+-x+}^{v'-v''} \right) \tau_{b+,v'} \tag{9}$$

where the emission is considered to be from the entire system.

Dividing Eq. 6 by Eq. 8 and substituting in Eq. 9 we get

$$N_{x+,v=0} = \left[\frac{\left\langle \sigma_{x+}^{e^-} v \right\rangle}{\left\langle \sigma_{b+}^{e^-} v \right\rangle} \right] \tau_{x+} \frac{E_{b+}}{T} F_{x+-x}^{0-0} \tag{10}$$

The following values are used for the quantities on the right hand side of Eq. 10:

$$\begin{aligned}
\left\langle \sigma_{X+}^{e^-} v \right\rangle / \left\langle \sigma_{B+}^{e^-} v \right\rangle &= 4.3 \quad \text{(calculated using diff. cross sections from Ref. [8])} \\
\tau_{x+} &= 4.4\,\text{msec} \quad \text{(at 100 km)(see Table 2 below)} \\
\tau_{B+} &= 90\,\text{nsec} \quad \text{(primarily radiative)} \\
E_{B+} &= 80 \text{ kiloRayleighs} \\
T &= 10 \text{ km} \\
F_{x+-x}^{0-0} &= 0.09
\end{aligned}$$

The density of $N_2^+(X^2\Sigma_g^+, v=0)$ is then

$$N_{x+,v=0} = 1.4 \times 10^2 \text{ cm}^{-3}.$$

5 Signal, Noise, and Signal to Noise Ratio

5.1 Signal

Here we present the results of calculations for the number of signal photons from 100 km for the four lidar scenarios depicted in Figure 3. The numbers of photons for the LIF lidars

	reaction	reaction time
1.	$N_2^+ + O_2 \longrightarrow N_2 + O^+$	6.50 msec
2.	$N_2^+ + O \longrightarrow NO^+ + N$	14.5 msec
3.	$N_2^+ + O \longrightarrow N_2 + O^+$	212 msec
4.	$N_2^+ + e^- \longrightarrow N + N$	900 sec

Table 2: Reactions primarily responsible for decay of N_2^+ at 100 km (T=200°K), and their reaction times. (From Ref. 9.)

are calculated using Eq. 2. The number of photons for the pump/LIF lidar is calculated using Eq. 4. The lidar parameters considered for these calculations are listed in Table 3.

The relevant absorption cross sections required for these calculations are listed in Table 4. The absorption cross sections are calculated using Eq. 3. Also shown in the table are transitions probabilities and linewidths. The linewidths are assumed to be due primarily to Doppler broadening. The temperature at 100 km is taken to be 200°K [11]. The transition probabilities are obtained from Ref. [12].

The relevant Franck-Condon factors required for these calculations are listed in Table 5. These values are obtained from Ref. [12].

Table 6 shows the number of photons detected per laser pulse in a 10 μsec time period from 100 km altitude during an IBC3 aurora for each of the lidar scenarios that we consider.

5.2 Uncertainties in the Signal

We consider four noise sources: 1) signal shot noise, 2) detector noise, 3) sky background, and 4) auroral background emission. The uncertainty (standard deviation) in the number of signal photons $n_{sig}(r)$ per laser pulse in one detector integration time period Δt is $\sigma_{sig} = n_{sig}^{1/2}(r)$.

The uncertainty in the number of effective photons n_{det} in a time period Δt due to detector noise is $\sigma_{det} = n_{det}^{1/2}$. For a photomultiplier tube n_{det} can be calculated from the dark current i_d, which is a quantity typically specified with a tube:

$$n_{det} = \frac{i_d \Delta t}{eG} \quad \text{(PMT)} \tag{11}$$

where e is the electron charge and G is the gain of the dynode chain.

The uncertainty in the number of sky background photons n_{sky} is $\sigma_{sky} = n_{sky}^{1/2}$. The

$E_o =$	100 mJ (dye laser)
	10 mJ (nitrogen laser)
	2 J (Nd:YAG laser)
	2.5 J (Ti:Sapphire laser)
	1 J (Nd:YLF laser)
$D_r =$	1 m
$\theta_r =$	0.5 mrad
$\Delta t =$	10 μsec
$\Delta\lambda =$	10 Å
$\eta =$	0.3 (1^{st} neg, 2^{nd} pos)
	0.1 (1^{st} pos)
$K =$	0.2 (1^{st} neg, 2^{nd} pos)
	0.3 (1^{st} pos)
$r =$	100 km
$T(r) =$	0.28 (2^{nd} pos)†
	0.5 (1^{st} neg)†
	0.8 (1^{st} pos)†

†Calculated with LOWTRAN [10]

Table 3: Lidar parameters used for the lidar signal calculations.

number of sky background photons detected in a time period Δt is

$$n_{sky} = \eta K \frac{B_\lambda \lambda}{hc} A \Omega \Delta\lambda \Delta t \tag{12}$$

where B_λ is the sky background spectral radiance at wavelength λ, Ω is the receiver field of view solid angle, $\Delta\lambda$ is the receiver bandwidth, η is the detector quantum efficiency, and K is the transmissivity of the receiver optics. The lidars we consider can, at best, operate during a moonlit night for which $B = 2.5 \times 10^{-9}$ W/m^2-ster-Å [13].

Nitrogen molecules which are excited directly, by auroral electron impact, to the upper state of the fluorescence transition may radiatively decay and be detected by the lidar

	1^{st} pos (2-0)	1^{st} pos (4-5)	2^{nd} pos (0-0)	1^{st} neg (1-0)
A (sec^{-1})	4.4×10^{4}	7.84×10^{3}	1.39×10^{7}	9.64×10^{6}
$\Delta\nu$(200°K) (GHz)	0.74	0.54	1.7	1.5
σ^a (cm^2)	1.43×10^{-14}	6.55×10^{-15}	3.70×10^{-13}	3.92×10^{-13}

Table 4: Transition probabilities, doppler linewidths, and photoabsorption cross sections used for the lidar signal calculations.

1^{st} pos (2-0)	1^{st} pos (4-2)	2^{nd} pos (0-0)	1^{st} neg (0-0)
0.1617	0.2976	0.4527	0.6481

Table 5: Franck-Condon factors used for lidar signal calculations.

laser	LIF 1^{st} pos	LIF 2^{nd} pos (0-0)	LIF 1^{st} neg (0-0)	pump (1^{st} pos (0-0))-LIF (2^{nd} pos (0-0))
nitrogen:	0.019	9×10^{-7}	0.0024	–
dye:	0.056	1.7×10^{-6}	0.0047	0.30†
Nd:YAG:	0.15	–	–	–
Nd:YLF:	–	–	–	3.0†
Ti:Sapphire:	1.4	–	0.0094	–

†Numbers appear in pump laser row. LIF laser is nitrogen.

Table 6: Number of photons detected per laser pulse for all lidars considered.

receiver. These photons constitute unwanted background, which we refer to as auroral background emission. The uncertainty in the number of auroral background emission photons n_{aur} is $\sigma_{aur} = n_{aur}^{1/2}$. The number of auroral background emission photons detected in a time period Δt is

$$n_{aur} = \eta K \frac{\pi}{4} E_{e'-e''}^{v'-v''} G \frac{\pi^2}{16} \theta_r^2 D_r^2 \Delta t T_d(r) \tag{13}$$

where $E_{e'-e''}^{v'-v''}$ is the column emission rate (in Rayleighs) due to transitions from the electronic/vibrational state e'/v' to e''/v'', G is the fraction of these photons that is within the bandwidth of the receiver (see discussion in Section 2), and all other quantities have the usual definitions.

Table 7 below shows the the number of sky background photons (moonlit night) and the number of auroral background emission photons detected in a time Δt.

	1^{st} pos (2-0)	1^{st} pos (4-2)	2^{nd} pos (0-0)	1^{st} neg (0-0)
auroral emission† (kR)	53.8	70.8	24.4	50
auroral emission (# photons)	0.35	0.21	0.31	0.74
sky bkgrnd (# photons)	0.009	0.009	0.008	0.009

Table 7: Number of sky background photons and auroral background emission photons in time Δt.

If all noise processes are statistically independent of each other then the total uncertainty σ_n in the number of photons for one laser pulse is

$$\sigma_n = \sqrt{\sigma_{sig}^2 + \sigma_{sky}^2 + \sigma_{det}^2 + \sigma_{aur}^2} = \sqrt{n_{sig}(r) + n_{sky} + n_{det} + n_{aur}} \tag{14}$$

For m laser pulses each photon number is multiplied m.

5.3 Signal/Noise

The signal to noise ratio $(S/N)_m$ for m laser pulses is

$$\left(\frac{S}{N}\right)_m = \frac{m^{1/2} n_{sig}(r)}{\sqrt{n_{sig}(r) + n_{sky} + n_{det} + n_{aur}}} \tag{15}$$

The following table shows the signal to noise ratios (for one laser pulse), for all the lidars considered, using Eq. 15 and the information and parameters presented in this section.

laser	LIF 1^{st} pos	LIF 2^{nd} pos (0-0)	LIF 1^{st} neg (0-0)	pump (1^{st} pos (0-0))-LIF (2^{nd} pos (0-0))
nitrogen:	0.031	2×10^{-6}	0.0024	–
dye:	0.087	3.0×10^{-6}	0.0054	0.38†
Nd:YAG:	0.24	–	–	–
Nd:YLF:	–	–	–	1.6†
Ti:Sapphire:	1.1	–	0.011	–

†Numbers appear in pump laser row. LIF laser is nitrogen.

Table 8: Signal to noise ratios for one laser pulse $(S/N)_1$ for all the lidars considered.

The signal to noise ratio scales with the parameters in the following way:

- Auroral background fluorescence limited:

$$\left(\frac{S}{N}\right)_m \propto (m\eta K \Delta r)^{1/2} \lambda E_o D_r \frac{N_{e,v}}{\left(E_{e'-e''}^{v'-v''}\right)^{1/2}}$$

- Shot noise limited:

$$\left(\frac{S}{N}\right)_m \propto (m\eta K \Delta r \lambda E_o N_{e,v})^{1/2} D_r$$

6 Conclusions

We have described two types of molecular nitrogen fluorescence lidars which can be used to determine excited or ionized N_2 density in the auroral ionsphere. In addition, the lidars can be used for high spatial resolution diagnostics during ionospheric high power radio frequency heating experiments which are often performed during moderate aurora. The first lidar is a conventional LIF lidar which operates in the first postive system of N_2 or the first negative system of N_2^+. Several different lasers are considered. The choice of laser determines the bands of excitation and fluorescence. The second lidar is a pump/LIF lidar. Two lasers are utilized. The first laser pumps N_2 from $A^3\Sigma_u^+$ to $B^3\Pi_g$ ((0-0) band, 10477 Å). The second laser then does LIF on the second positive system ((0-0) band, 3371 Å).

We have calculated the signal to noise for both types of lidars using reasonable lidar parameters. We have considered four noise processes: 1) signal shot noise, 2) auroral background emission, 3) ambient sky background, and 4) detector noise. We have considered several different electronic systems of N_2 and N_2^+ (1^{st} pos, 2^{nd} pos, 1^{st} neg) and several different lasers.

The most promising lidars are

1. A LIF lidar operating in the 1^{st} positive system (2-0) band, using a tunable Ti-Sapphire laser. The signal to noise for one laser pulse is $(S/N)_1 = 1.1$. Required averaging time for $S/N = 100$ is 165 sec (at 50 Hz).

2. A LIF lidar operation in the 1^{st} positive system (4-5) band, using a seeded Nd:YAG laser (tunable over ≈ 1 Å). For this lidar $(S/N)_1 = 0.24$. Required averaging time for $S/N = 100$ is 5790 sec (at 30 Hz).

3. A pump/LIF lidar using a Nd:YLF laser as a pump in the 1^{st} positive system and a dye laser for LIF in the 2^{nd} positive system. For this lidar $(S/N)_1 = 1.6$. Required averaging time for $S/N = 100$ is 130 sec (at 30 Hz).

The pump/LIF lidar is preferable to the conventional LIF lidar since higher signal to noise ratios can be achieved. The primary reason for this is that the signal is proportional to the square of the inverse of the divergences of the lasers. The divergences can be made very small with the use of beam expanders.

The conventional LIF lidar is preferrable in the short term since it utilizes only a single laser. It is easier to adapt an existing Rayleigh lidar to become a LIF lidar. Utilizing a dye

laser for this type of lidar is preferable since the highest signal to noise ratio can be achieved. However, since many Rayleigh lidars use high power Nd:YAG lasers, it is straightforward to convert such a lidar into a LIF lidar as described in this report. All that is required is a new filter and a new photomulitplier tube in the receiver. The nitrogen laser approach for the conventional LIF lidar is attractive since no tuning is required. However, this desirable feature is offset by the low power. There is a question as to availability of a first positive nitrogen laser.

Appendix A Wavelength Calculations

All wavelengths presented in this report are calculated theoretically in the manner described here.

A rotational level of a diatomic molecule such as N_2 and N_2^+ is specified by its term energy $T = E/hc$, where E is the energy. The term energy of a rotational level can be written as

$$T = T_o + G(v) + F_v(J) \tag{16}$$

where T_o is the electronic term, $G(v)$ is the vibrational term, and $F_v(J)$ rotational term. v and J are the vibrational and rotational quantum numbers, respectively. In general, the rotational term is a function of the vibrational quantum number as well as the rotational quantum number.

The vibrational and rotational terms are written as series in the vibrational and rotational quantum numbers respectively:

$$G(v) = \omega_e(v+1/2) - \omega_e x_e(v+1/2)^2 + \omega_e y_e(v+1/2)^3 + \omega_e z_e(v+1/2)^4 + \cdots \tag{17}$$

$$F_v(J) = B_v J(J+1) - D_v J^2(J+1)^2 + H_v J^3(J+1)^3 + \cdots \tag{18}$$

where

$$B_v = B_e - \alpha_e(v+1/2) + \gamma_e(v+1/2)^2 + \delta_e(v+1/2)^3 + \cdots \tag{19}$$

$$D_v = D_e + \beta_e(v+1/2) + \cdots \tag{20}$$

$$H_v = H_e + \cdots \tag{21}$$

The quantities

$$\omega_e,\ x_e,\ y_e,\ z_e,\ B_e,\ D_e,\ H_e,\ \alpha_e,\ \gamma_e,\ \delta_e,\ \beta_e$$

are spectroscopic constants which can be looked up in tables. We use tables from Ref. [7].

The wavelength of radiation resulting from a radiative decay between two rotational levels is

$$\lambda = \frac{1}{T_u - T_l} \tag{22}$$

where T_u and T_l are the term energies for the upper and lower transition levels respectively. All wavelengths in this report are calculated using Eq. 22 with Eqs. 16 to 18. Calculated wavelengths have uncertainties due to uncertaintes in spectroscopic constants and unavailability of some constants. Uncertainties may be, at most, on the order of a few tenths of an Angstrom.

Appendix B Tests at UCLA Plasma Physics Laboratory

B.1 Introduction

In February, 1993 one of the authors (Garner) spent two weeks at the UCLA Plasma Physics Laboratory (UCLA PPL) as part of a collaborative effort between Phillips Laboratory (Geophysics Directorate, GPIM branch) and UCLA PPL to study the feasibility of a molecular nitrogen fluorescence lidar as a diagnostic for high power rf heating experiments of the ionosphere. The specific purpose of the visit was to investigate laser induced fluorescence of the first positive system of N_2 in a laboratory based nitrogen plasma to determine its feasibility as the basis for a lidar. The GPIM branch supplied a dye laser for these studies. UCLA PPL personnel directly involved in the effort were Dr. Ralph Wuerker, Mr. Tetsuo Fukuchi, and Dr. Alfred Wong. The general laboratory facilities and support personnel were available as well.

The results of the experiments were inconclusive. We were not successful in demonstrating laser induced fluorescence of the first positive system. We discuss possible reasons for this below. Additional experimentation is required.

The UCLA PPL has an ongoing research program aimed at investigating the spectroscopy of N_2 and N_2^+ in laboratory simulations of ionospheric plasmas. During this research they have successfully demonstrated laser induced fluorescence in the the second positive system of N_2 and the first negative system of N_2^+ [14]. They do not have a laser suitable for excitation in the first positive system. For the second positive system they used a nitrogen laser operating in the (0–0) band at 3371 Å and detected fluorescence in the same band and from several other bands with upper vibrational level $v = 0$. For the first negative system they used, in different experiments, a nitrogen laser and a dye laser laser. Both lasers operated in the in the (1–0) band at 4278 Å. The dye laser operated at a specific rotational level within the band. In these LIF experiments they measured lifetimes of the observed fluorescence transitions and absorption cross sections of the excitation transitions. For the first negative system they compared the relative merits of wide band excitation (nitrogen laser) and narrow band excitation (dye laser).

Our calculations, presented in this report, indicate that the first positive system of N_2 may be more promising for lidar use than the other systems. Therefore, we set out, with the UCLA PPL group, to demonstrate first postive laser induced fluorescence. Specifically, we

set out to demonstrate the first scenario depicted in Figure 3. In one part of that scenario a dye laser is used to excite the transition $N_2(A^3\Sigma_u^+, v=0, J=6) \longrightarrow N_2(B^3\Pi_g, v=2, J=5)$. The wavelength is theoretically (see Appendix Appendix A) 7737 Å. Fluorescence radiation is then detected from one or all three of the branches of the reverse transition. The (2–0) band of the first positive system offers the best combination of wavelength, cross section, and Franck-Condon factor for lidar use (see discussion in Section 2.1). The $J = 5$ rotational level is expected to be the most abundant rotational level at 100 km (200°K).

The specific goals of the work at UCLA PPL included

- set up and operate the GPIM dye laser in a wavelength regime suitable for probing the (2–0) band of the first positive system (750-800 nm),
- determine the precise wavelengths of the rotational lines of this band,
- determine the radiative lifetimes of the laser excited states,
- determine the linewidths of the fluorescence transtions,
- determine the photoabsorption cross sections (using the above measurements),
- re-evaluate first positive LIF lidar performance with these results, and
- evaluate the performance of a first positive LIF lidar utilizing the same dye laser in the GPIM mobile lidar system at the HIPAS observatory.

B.2 Description of Experiment

Figure 4 shows the experimental setup. The GPIM dye laser is pumped with a UCLA PPL XeCL excimer laser. The laser output is routed to the plasma chamber, located in a different room in the facility. The total optical path is approximately 35 m. The light is directed through a window at the center of the top of the cylindrically shaped chamber. The light travels through the chamber along the diameter of the cylinder, through another window at the bottom, and hits a photodiode. A spectrometer is located on the side of the chamber so as to detect fluorescence radiation at 90° scattering angle from the optic axis.

The dye laser is a Lambda Physik model FL2002E. This laser contains an oscillator and preamplifier sections which use one dye cuvette, and a main amplifier section which uses a second cuvette. We operated this laser with a variety of dyes during the course of the

Laboratory Experiments at UCLA PPL (8-19 Feb 1993)

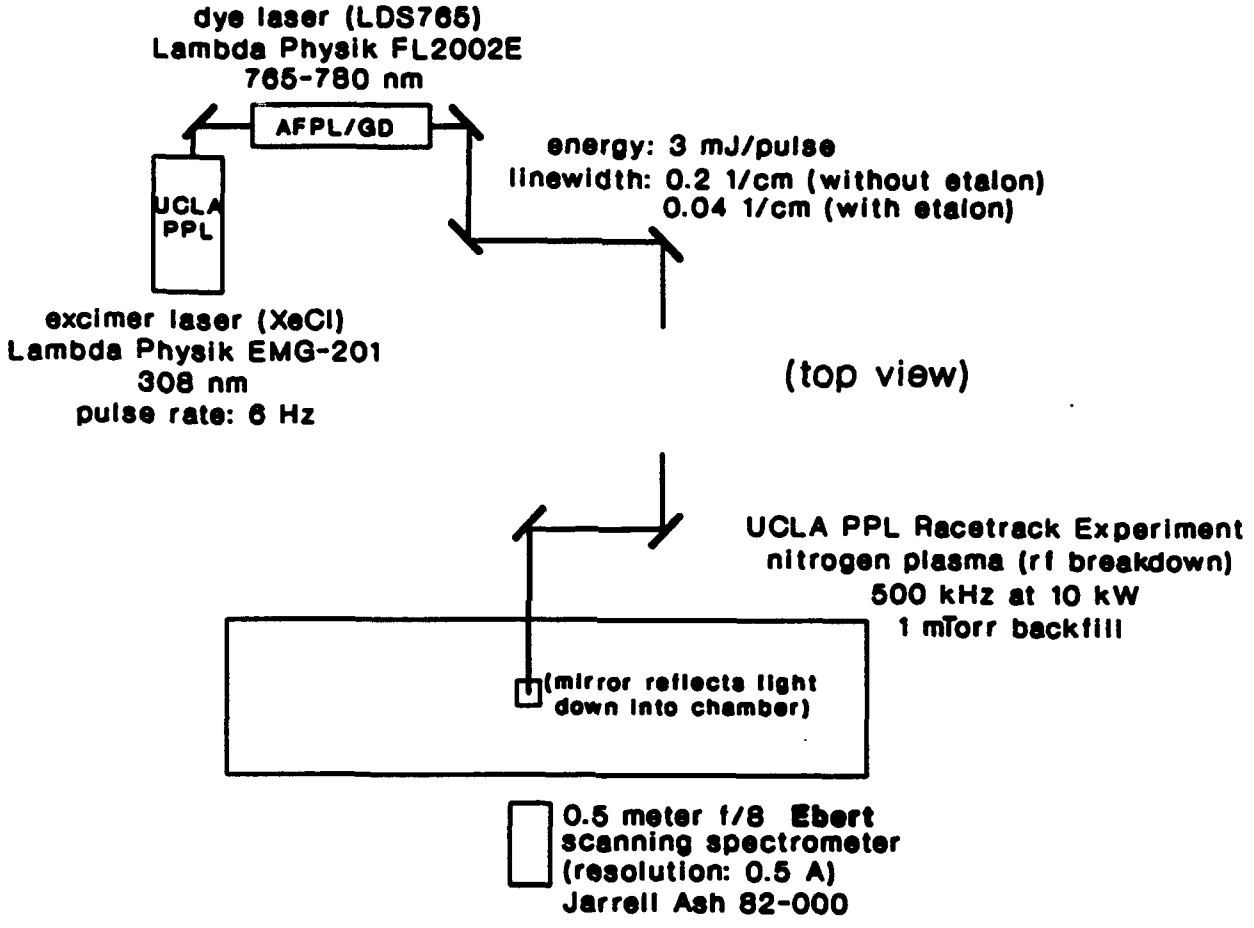

Figure 4: Experimental setup of laser induced fluorescence experiments on UCLA PPL Racetrack rf plasma chamber.

experiment in order to find the one that provided for the most energy in the wavelength regime of interest. The dye which we found most suitable was LDS765 (Exciton). With this dye in both the oscillator/preamplifier and amplifier cuvettes we obtained 2.5-3 mJ/pulse in the range 760-780 nm. We obtained 1-2.5 mJ/pulse in the range 740-760 nm. These energies were obtained without the use of the manufacturer-supplied intracavity etalon in the oscillator. With the etalon the energies were approximately 10% of these values. According to the manufacturer's specifications, the etalon reduces the laser linewidth from 0.2 cm^{-1} to 0.04 cm^{-1}. As a comparison, the linewidth of a N_2 first positive rotational line at 200°K is 0.025 cm^{-1}.

The excimer laser used to pump the dye laser is a Lambda Physik model EMG-201 operating with XeCl at 308 nm. The output energy, which produced the dye laser energies cited above, was 75 mJ/pulse. The pulse repetition rate was 6 Hz.

Most of the experiments were performed on nitrogen plasmas produced in the UCLA PPL Racetrack Experiment. Nitrogen plasmas are created by rf breakdown of N_2 gas. The gas is backfilled into the chamber to pressures in the range of 10^{-4} to 10^{-3} Torr. Different pressures produce different plasma conditions. Most of the experiments were performed with 10^{-3} Torr backfill. Approximately 10 kW of rf energy at 500 kHz is delivered by an antenna located inside the chamber. The rf is pulsed at 6 Hz, in synchronization with the excimer laser. Some experiments were performed in the UCLA PPL Torch experiment. In this experiment N_2 can be backfilled into the chamber to as much as 1 Torr, producing much higher density plasmas than in Racetrack.

The spectrometer used to detect fluorescence radiation is a Jarrell Ash model 82-000. This is a 1/2 meter, f/8 Ebert type spectrometer (uses a grating). The minimum resolvable wavelength difference in the 740-780 nm range is approximately 0.5 Å.

The detector was a photomultiplier tube operating in current mode. The output of the PMT was directed to a Tektronix digitial oscilloscope with 200 MHz maximum digitization rate and averaging capability.

B.3 Experimental Technique

The first major task after setting up the dye laser to operate suitably in the (2–0) band of the first positive system, was to observe laser induced fluorescence. Since the wavelengths were calculated theoretically a detailed wavelength scan of the laser was required.

Our technique for observing laser induced fluorescence followed the following steps:

1. Tune the dye laser wavelength through the (2-0) band, from 740 nm to 790 nm, in steps of 0.003 Å. We expect this step size to be more than adequate. The laser linewidth is approximately 0.2 cm^{-1}, or 0.1 Å at 7737 Å, without the etalon. The linewidth of the rotational lines of the neutral molecules in the experiment was about 0.03 cm^{-1}, or 0.02 Å at 7737 Å (doppler spread at room temperature). The separation between rotational lines in the first positive system is on the order of several tenths of Å.

2. Observe (wall) scattered laser radiation with the spectrometer set for widest pass band, $\sim$ 10 Å. Doing this assures us that the spectrometer is set for the same wavelength as the laser. The signal from the scattered radiation is approximately 10 nsec in duration, the laser pulse width.

3. Shift the spectrometer center wavelength as the laser wavelength is scanned.

4. Observe the fluorescence signal due to the decay of the molecule via the reverse pathway of the laser excited transition. The signal from fluorescence should add an exponentially decaying tail to the signal from wall scattered radiation. The tail should have a time constant equal to the radiative lifetime of the upper state of the fluorescence transition ($\sim$ 10 μsec).

5. If the previous step is successful, then with the same excitation wavelength observe fluorescence in other branches of the same band and in other bands (e.g., the (2-1) band which has band head at $\lambda \sim$ 8695 Å).

6. Continue with the wavelength scan to map out the rotational structure of the (2–0) band.

With the above data lifetimes, linewidths, temperatures, and absorption cross sections can be determined. Lifetimes and linewidths come directly from the fluorescence signals. Temperatures are determined by either calculating from the linewidths of individual rotational lines or by considering the relative strengths of signals from different rototional lines. The latter gives the rotational temperature. Cross sections are determined using Eq. 3, with transition probability (inverse of lifetime) and linewidth from the data.

B.4 Results and Conclusions

As mentioned above, we were not successful in demonstrating laser induced fluorescence in the first positive system. We do not have a definitive explanation for this, although we cite some possible reasons.

- There may be less $N_2(A)$ than we expect in the Racetrack experiment. This, of course, should have no bearing on experiments performed in the ionosphere. We estimate $N_2(A^3\Sigma_u^+)$ density in the aurora from direct observations (see Section 4).
- The background fluorescence may have been too high. If this is the case then it is necessary to average over more laser pulses. We averaged over as many as twenty pulses.
- The absorption cross section is lower than we expect. This is the only reason we cite which would also affect our lidar calculations in this report.

We have some evidence that suggests the first reason cited above may be the real reason. We compare expected spectrometer signals from second positive LIF and first positive LIF. Second positive LIF was observed in the Racetrack experiment. The ratio of spectrometer signals is given by

$$\frac{P_{7737}}{P_{3371}} = \left(\frac{N_{A,0}}{N_{B,0}}\right)\left(\frac{R_{A,J}}{R_{B,J}}\right)\left(\frac{\mathcal{L}_{AB}(\lambda)}{\mathcal{L}_{BC}(\lambda)}\right)\left(\frac{(\eta K)_{7737}}{(\eta K)_{3371}}\right)\left(\frac{\sigma_{AB}}{\sigma_{BC}}\right)\left(\frac{\tau_{BC}}{\tau_{AB}}\right)\left(\frac{F^{2-0}_{B-A}}{F^{0-0}_{C-B}}\right)\left(\frac{E_{oA}}{E_{oB}}\right)$$

$$= \left(\frac{N_{A,0}}{N_{B,0}}\right)\left(\frac{0.1}{0.05}\right)\left(\frac{0.1}{1}\right)\left(\frac{0.1}{0.3}\right)\left(\frac{1.43\times10^{-14}}{3.7\times10^{-13}}\right)\left(\frac{90\times10^{-9}}{9\times10^{-6}}\right)\left(\frac{0.1617}{0.4527}\right)\left(\frac{3}{6}\right)$$

$$= \left(\frac{N_{A,0}}{N_{B,0}}\right)\times 4.1\times10^{-6}$$

where we have substituted probable values for each of the quantities.

If the first positive signal to be equal to the second positive signal then Racetrack must have 2.4×10^5 times as many $N_2(A^3\Sigma_u^+)$ as $N_2(B^3\Pi_g)$. This may not be the case in the experiment. In any case, if there are only a small number of $N_2(A^3\Sigma_u^+)$ that simply implies a small signal in which case more sensitivity is required of the detector/data acquisition system (e.g., averaging over more shots).

We know that the laser was scanning the correct wavelength regime. Figure 5 shows passive emission from the plasma as a function of wavelength. The data was acquired with

the spectrometer near the end of the rf pulse. The spectrometer was set for approximately 1 Å resolution. Data was averaged over four shots. Different bands are clearly discernable. However individual rotational lines are not resolved.

Appendix C Auroral Emission Data Acquired at HIPAS, Alaska

During the autumn of 1992 and winter of 1993 passive emission from aurora was observed using the receiver of the Phillips Laboratory (Geophysics Directorate, GPIM branch) mobile lidar system at HIPAS observatory in Alaska. The overall purpose of these observations was to evaluate the lidar receiver performance in possible LIF lidar wavelength regimes (e.g., 7737 Å, 4278 Å, 3914 Å). The specific goal of these observations were

- to acquire data with the lidar receiver during aurora at different wavelengths,
- correlate with measurements from calibrated photometers operating at 3914 Å,
- estimate lidar sensitivity at potential LIF wavelengths, and
- re-evaluate previous LIF lidar calculations.

To date several data sets have been acquired.[5] Figures 6 and 7 show two sets of data. The first figure shows emission at 774 nm and the second figure shows emission at 428 nm. The bandpass for both cases is 10 nm. Both figure show plots of, as a function of time, the number of photons collected per second (left hand side) or the column emission rate in Rayleighs (right hand side). The data is cut off as the photon count rate increases because of sunrise. Both plots indicate emission activity above background, although much lower than even a weak aurora would produce.

[5]Data was acquired by Richard Dickman of the HIPAS observatory and by Ralph Wuerker of UCLA PPL.

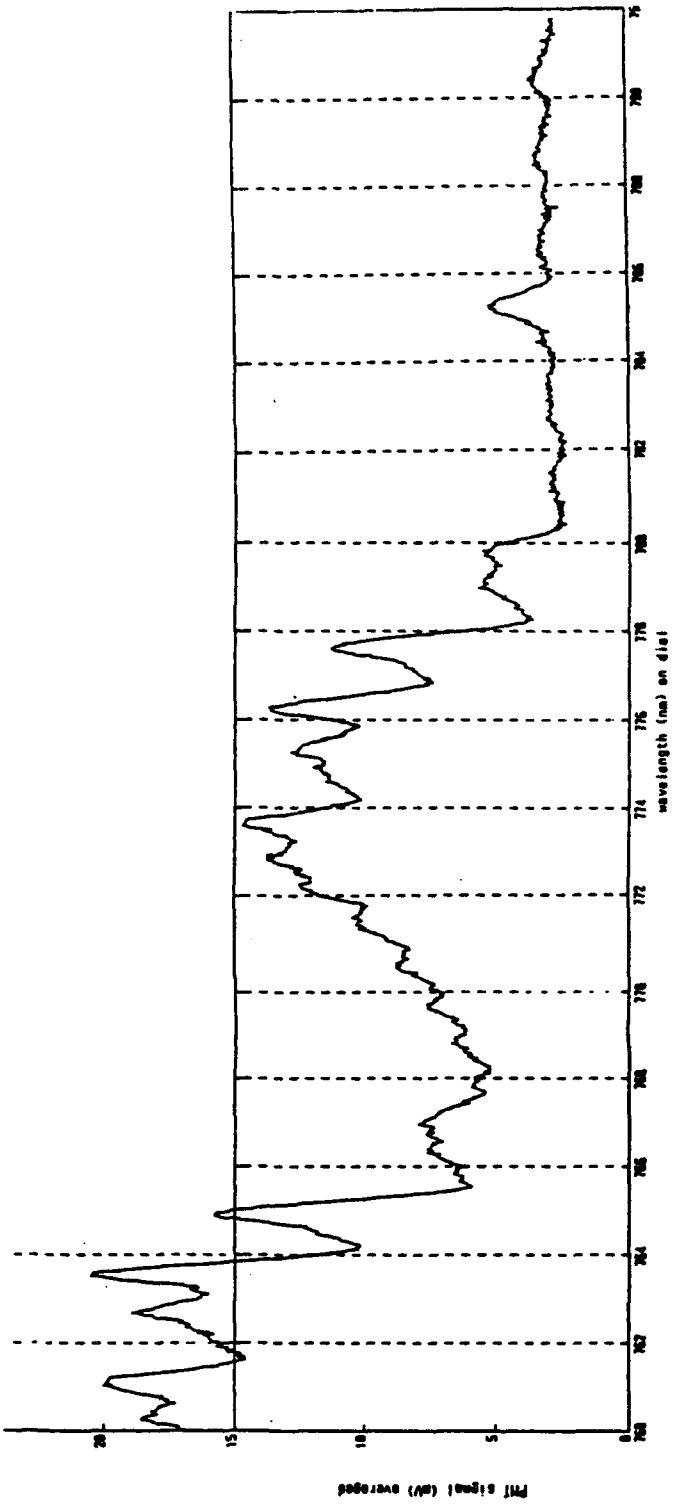

Figure 5: Passive emission as a fuction of wavelength in the first positive system from the UCLA PPLA Racetrack plasma.

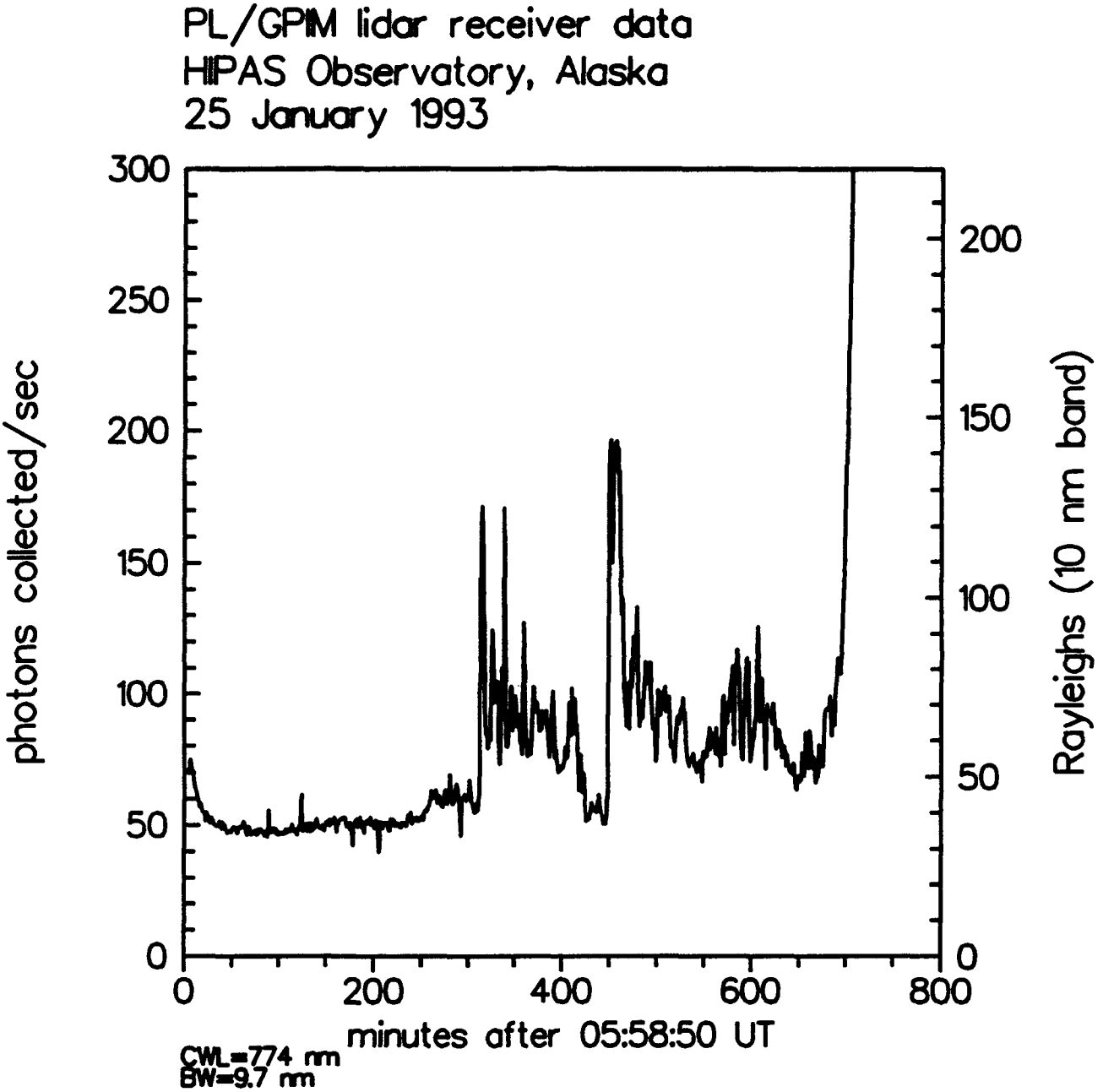

Figure 6: Passive emission at 774 nm recorded by the GPIM lidar receiver at HIPAS observatory.

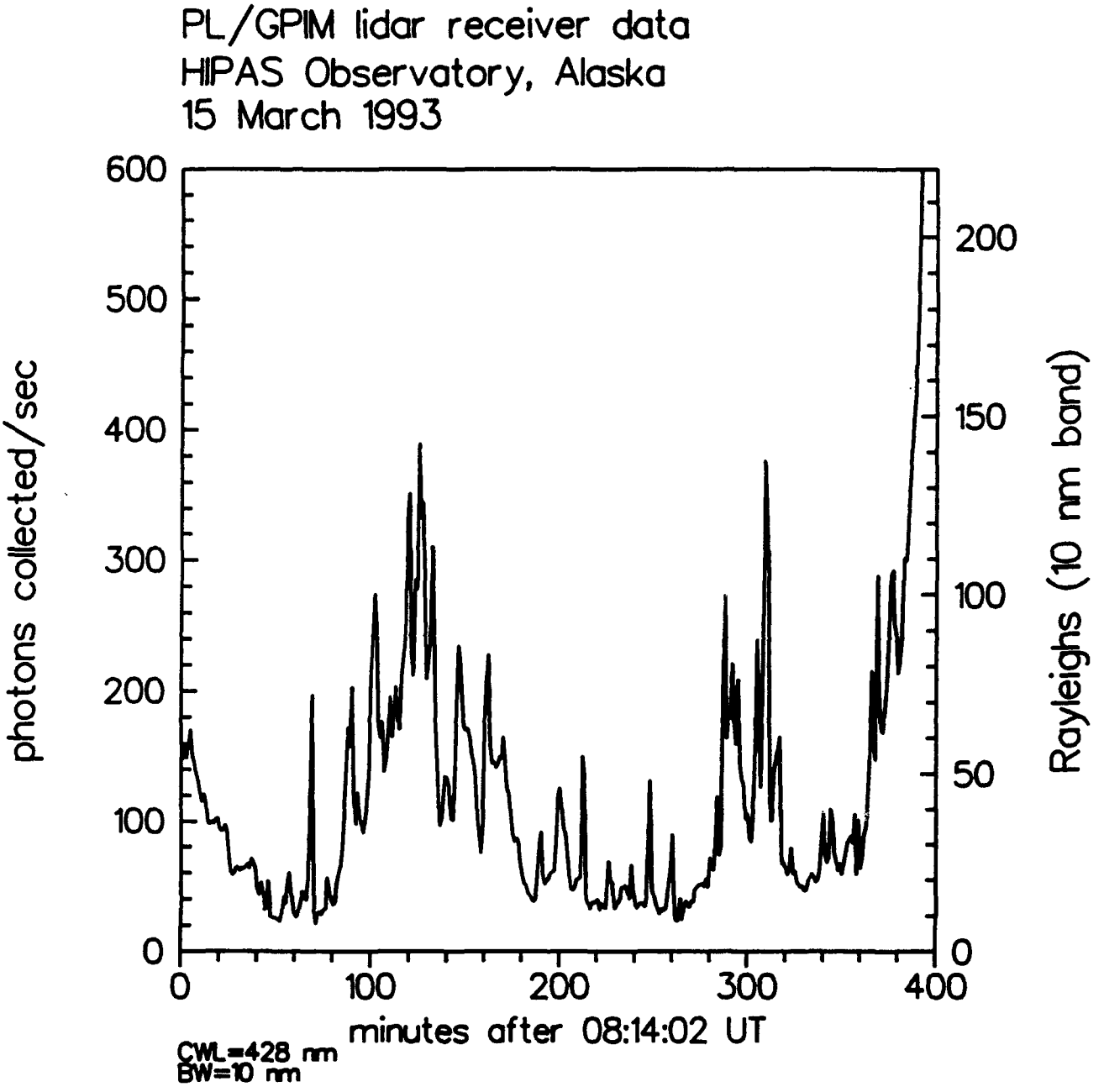

Figure 7: Passive emission at 428 nm recorded by the GPIM lidar receiver at HIPAS observatory.

References

[1] Private communciation, Dr. Ralph Wuerker, UCLA Plasma Physics Laboratory, Los Angeles, CA.

[2] The idea of using a nitrogen laser for nitrogen fluorescence lidar was first proposed to us by Dr. Alfred Wong, UCLA Plasma Physics Laboratory, Los Angeles, CA.

[3] M. Burka, P. Dao, G. Davidson, R. Farley, J. Meriwether, and A. Wilson, "Elastic and Raman Lidar Temperature Measurements from Poker Flat, Alaska, During February 1992," *Procedings of the 16th International Laser Radar Conference*, NASA CP 3158, 333-336, 1992.

[4] J.W. Wright, H. Kopka, and P. Stubbe, "A Large-Scale Ionospheric Depletion by Intense Radio Wave Heating," *Geophys. Res. Lett.* **15** (13), 1531–1533, (1988).

[5] A. Vallance Jones, "Auroral Spectroscopy," *Space Science Reviews* **11**, 797 (1971).

[6] R.M. Measures, *Laser Remote Sensing*, John Wiley & Sons (1984).

[7] G. Herzberg, "Spectra of Diatomic Molecules," 2nd edition, Van Nostrand Reinhold Company, New York (1950).

[8] H.T. Wadzinski and J.R. Jasperse, "Low Energy Electron and Photon Cross Sections for O, N_2, and O_2, and Related Data," Report #AFGL-TR-82-0008, Space Physics Division, Air Force Geophysics Laboratory, Air Force Systems Command, USAF, Hanscom AFB, MA, 1982. ADA118921.

[9] Defense Nuclear Agency Reaction Rate Handbook, second edition, March 1972.

[10] PC-Tran, Version 7 (Lowtran computer program for the PC), Ontar Corporation.

[11] "U.S. Standard Atmosphere, 1976," National Oceanic and Atmospheric Administration, National Aeronautics and Space Administration, and U.S. Air Force, Washington, D.C. (1976).

[12] A. Lofthus and P.H. Krup, "The Spectrum of Molecular Nitrogen," *Journal of Physical and Chemical Reference Data* **6**, (1977).

[13] R. Kauth, *Handbook of Military Infrared Technology (Chapter 5: Backgrounds)*, edited by W.L. Wolfe, Office of Naval Research and Department of the Navy, Washington, D.C. (1965).

[14] R.F. Wuerker, L. Schmitz, T. Fukuchi, and P. Strauss, "Lifetime Measurements of the Excited States of N_2 and N_2^+ by Laser-Induced Fluorescence," *Chem. Phys. Lett.* **150**, 443-446, 1988.